The 9th European Congress on Computational Methods in Applied Sciences and Engineering
ECCOMAS Congress 2024
3 – 7 June 2024, Lisboa, Portugal

WAVELET ANALYSIS FOR THE VERTICAL ISOLATION RATIO OF RC HOSPITAL STRUCTURES SUBJECTED TO NEAR-FAULT EARTHQUAKES

FABIO MAZZA[*], ANDREA BRAILE[*] AND RODOLFO LABERNARDA[*]

[*] Dipartimento di Ingegneria Civile (DINCI)
Università della Calabria
Ponte P. Bucci, 87036, Rende (Cosenza), Italy
e-mail: fabio.mazza@unical.it
e-mail: andrea.brail97@gmail.com
e-mail: rodolfo.labernarda@unical.it

Key words: RC framed structure, Vertical isolation ratio, Near-fault vertical ground motion, Nonlinear dynamic analysis, Wavelet analysis.

Summary. It is recognized that the purely elastomeric and frictional bearings cannot provide effective vertical seismic isolation of a framed structure due to their high vertical frequency. Amplification of the vertical acceleration along the building height is documented in the near-fault area. Moving resonance effects in the vertical direction are also expected due to shifting of the dominant vibration periods related to the nonlinear behaviour of both the superstructure and base-isolation system. New seismic isolation systems able to carry the gravity loads with relatively low vertical stiffness have been proposed, but the calibration of the vertical isolation ratio remains elusive. The main objective of this work is to evaluate the isolation ratio in the vertical direction required for effective protection against the vertical component of near-fault ground motions. To this end, the horizontal and vertical base-isolation is applied to an existing five-storey RC pavilion of the hospital campus in Avellino (Italy). An in-series vertical assembly of a high-damping rubber bearing (HDRB) and a high-damping rubber layer (HDRL), the latter independent of the horizontal and vertical (in tension) responses of the HDRB, is adopted. Design properties of the HDRBs are evaluated in line with provisions of the European seismic codes, while thickness of the HDRLs corresponds to eight values of the vertical-to-horizontal stiffness ratio used for the base-isolated test structures. A purpose-built C++ code adopts a lumped plasticity model for RC frame members and coupling of the horizontal and vertical motions, change of the critical buckling load due to significant horizontal displacement and cavitation for the HDRBs. A purpose-built Matlab code is implemented to investigate effects of the time-varying structural response on the vertical seismic isolation, using the continuous wavelet transforms in combination to the complex Morlet wavelet. Elastic and inelastic dynamic time-history analyses are carried out in order to calibrate results of the wavelet analysis, considering a set of fifteen near-fault earthquakes with pulse-type behaviour in the horizontal and vertical directions. It is concluded that wavelet analysis represents a useful and simplified tool for an optimal selection of the vertical isolation ratio, requiring only results of elastic dynamic analysis of the test structure.

1 INTRODUCTION

Base isolation systems turned out to be very useful to enhance the seismic performance of buildings undergoing strong horizontal earthquakes, especially when medical facilities are considered [1]. One of the most widely employed type of isolators is the elastomeric one (e.g. High Damping Rubber Bearing, HDRB), but it is unable to provide effective vertical isolation because of the high vertical stiffness required to support gravity loads. The problem can be significantly impacting in the near-fault area, where notable values of the vertical-to-horizontal peak ground accelerations ratio happen together with an amplification of the corresponding spectral accelerations ratio in the range of low vibration periods [2]. Hence, the vertical acceleration may produce the formation of plastic hinges at the mid-span section of beams at the upper storeys, also influencing the functionality of nonstructural elements [3]. Moreover, vertical moving resonance effects may arise when the reduction of the dominant frequencies of a base-isolated structure, related to the nonlinear behaviour of both the superstructure and base-isolation system, matches the main frequency content of the vertical near-fault ground motion [4]. First attempts of horizontal and vertical base-isolation systems are proposed for structures of critical importance (e.g. nuclear power plant), where a combination of HDRBs and air and hydraulic springs is used [5]. In recent years, in-series combination of horizontal HDBR and inclined lead RB [6] and HDRB and HDR layers without tension force [7] are proposed for multi-storey buildings. A different solution is proposed in [8], where the in-elevation vertical flexibility is achieved by laterally restrained column bearings placed at discrete locations along the height of the building. Nevertheless, information is missing about the isolation ratio in the vertical direction providing effective protection against the notable vertical component of near-fault earthquakes.

The effects of the vertical stiffness variability of the isolation system are investigated in the present work, considering the horizontal and vertical base-isolation as retrofitting solution for a fixed-base five-storey RC pavilion of the hospital campus in Avellino (Italy). An in-series vertical assembly of a high-damping rubber bearing (HDRB) and a high-damping rubber layer (HDRL), the latter independent of the horizontal and vertical (in tension) nonlinear responses of the HDRB, is adopted as base-isolation system. Eight values of the vertical-to-horizontal stiffness ratio are selected, combining a HDRB designed in line with provisions of the European seismic codes with eight HDRLs of different thickness [9, 10]. Linear (LTH) and nonlinear (NLTH) time-history analyses of the fixed-base and base-isolated test structures are carried out by means of a purpose-built C++ code [11]. To this end, fifteen near-fault ground motions with pulse-type behaviour in the horizontal and vertical directions are selected on the basis of the variational mode decomposition technique [12] and extracted from the Pacific Earthquake Engineering Research center database [13]. A purpose-built Matlab code is developed to investigate vertical moving resonance effects, using the continuous wavelet transform in combination to the complex Morlet wavelet [14]. Finally, the optimal vertical isolation ratio is obtained combining wavelet analysis and LTH and NLTH results.

2 TEST STRUCTURES

A fixed-base (FB) five-storey RC pavilion of the hospital campus in Avellino (Italy), whose plan and elevation views are reported in Figure 1, is selected as test structure. It is designed in accordance to an old Italian seismic code [15] at the ultimate limit state, for a medium-risk

seismic zone and a typical subsoil class, and at the serviceability limit state, assuming a drift ratio threshold (Δ/h) equal to 0.4% (where Δ and h represent the interstorey drift and the storey height, respectively) with the purpose of limiting nonstructural damage of masonry infills. A cylindrical compressive strength of 25 MPa and a yield strength of 450 MPa are assumed for concrete and steel, respectively. Cross-section of beams and columns and seismic floor masses are reported in Figure 1 for the original (fixed-base) structure, leading to fundamental vibration periods $T_{FB,1X}$, $T_{FB,1Y}$ and $T_{FB,1Z}$ equal to 0.677s, 0.574s and 0.066s, respectively. Further information can be found in [16].

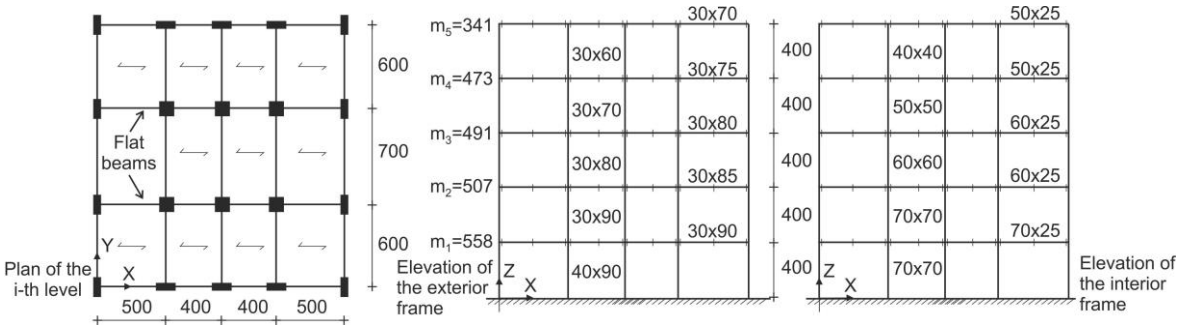

Figure 1: Plan and elevation views of the fixed-base RC building (units in kNs^2/m and cm)

Then, the retrofitting of the fixed-base building through base-isolation is designed for a high-risk seismic zone and moderately-soft subsoil class (i.e. class C, site amplification factors S_H and S_V equal to 1), accounting for both horizontal (PGA_H=0.499g) and vertical (PGA_V=0.476g) seismic loads in line with current Italian seismic code [17]. Specifically, horizontal (i.e. BIH) and horizontal and vertical (i.e. BIHV) base-isolated structures are considered (Figure 2), supposing that twenty identical HDRBs act alone and in vertical combination with twenty identical HDRLs with different vertical stiffness. It should be noted that floor masses of the superstructure differ from those of the fixed-base configuration, where 3 kN/m^2 is assumed for the likelihood of crowding on all floors [15], because of live loads correspond to different types of occupancy [17]: i.e. 3 kN/m^2 at the first and second levels (medical rooms); 2 kN/m^2 at the third and fourth levels (hospital rooms) and on the roof. A live load of 5 kN/m^2 (emergency area) is assumed for the ground level above the grid of rigid beams at the isolation level.

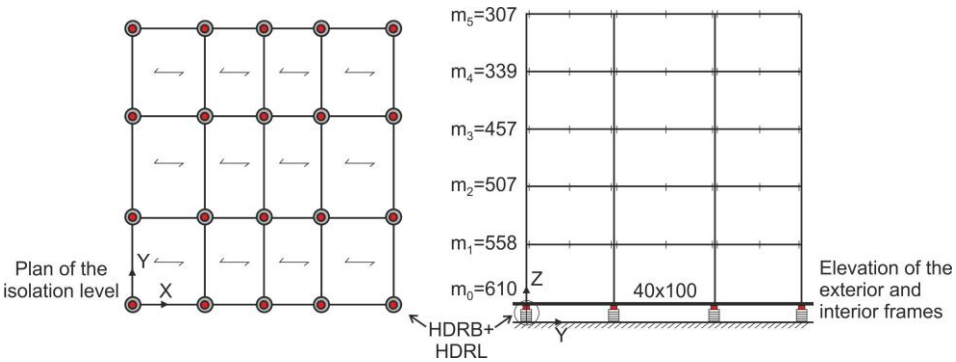

Figure 2: Plan and elevation geometry of RC building base-isolated along the horizontal (BIH) and horizontal and vertical (BIHV) directions (units in kNs^2/m and cm)

Upper- (UB) and lower-bound (LB) properties of the HDRBs are evaluated in accordance to European codes [9, 10]. Specifically, force at zero displacement (F_0) and post-elastic stiffness (K_p), corresponding to a simplified bilinear force-displacement law, are evaluated. To this end, different values of property modification and combination factors are assumed in order to take into account environmental and behavioural effects, so obtaining the following design factors: i.e. LB value equal to 0.8 for both F_0 and K_P; UB values equal to 1.55 and 1.75 for F_0 and K_P, respectively. For the sake of safety, a mixed design approach is used referring to LB strength and UB stiffness values.

The horizontal base-isolation system made of HDRBs is designed at the collapse prevention (CP) ultimate limit state, considering a volumetric compression modulus (E_b) and a shear modulus (G) of the elastomer equal to 2000 MPa and 0.5 MPa, respectively. The effective stiffness ratio of the isolation system (i.e. $\alpha_{Ke}=K_{eV,HDRB}/K_{eH,HDRB}$, defined as the ratio between the vertical and horizontal effective stiffnesses of the HDRB) is resulted equal to 2400. In particular, the following design provisions are fulfilled [10]: $\gamma_{tot}\leq 7$ and $\gamma_s\leq 2.5$, with γ_{tot} and γ_s representing the total and seismic shear strains of the elastomer, respectively; $P_{max}/P_{cr}\leq 0.5$, where P_{max} and P_{cr} represent the maximum compression axial load and the critical axial load, respectively; a ratio between the horizontal design displacement at the CP limit state (d_{dC}=35.2 cm) and the diameter of the internal steel reinforcing plates (D_l=66.5 cm) lower than 0.7; ultimate tensile strength of the elastomer (σ_{tu}) equal to 1 MPa and maximum compressive stress of steel plates ($\sigma_{s,max}$) lower than f_{yk} (275 MPa). Main design properties of the HDRBs are reported in Table 1: i.e. stiffness ratio (α_{Ke}); primary (S_1) and secondary (S_2) shape factors; critical axial load (P_{cr}); horizontal ($\xi_{eH,BI}$) and vertical ($\xi_{eV,BI}$) equivalent viscous damping ratios and corresponding horizontal ($C_{eH,HDRB}$) and vertical ($C_{eV,HDRB}$) viscous damping constants; horizontal ($K_{eH,HDRB}$) and vertical ($K_{eV,HDRB}$) effective stiffnesses. As a result, the horizontal ($T_{BI,1H}$) and vertical ($T_{BI,1V}$) fundamental vibration periods of the BIH structure are equal to 2.21s and 0.077s, respectively.

Table 1: Design properties of the horizontal base-isolation system with HDRBs (units in kN, m and s)

α_{Ke}	S_1	S_2	P_{cr}	$\xi_{eH,BI}$	$\xi_{eV,BI}$	$K_{eH,HDRB}$	$K_{eV,HDRB}$	$C_{eH,HDRB}$	$C_{eV,HDRB}$
2400	34.2	4.7	13559	0.079	0.050	131054	314530272	6700	61100

With the aim of obtaining the base-isolation also in the vertical direction, an in-series vertical arrangement of a HDRB and a HDRL, the latter independent of the horizontal and vertical (in tension) responses of the HDRB, is assumed. Eight values of the vertical-to-horizontal stiffness ratio of the BIHV structures are considered varying the thickness of the HDRLs, leading to the main design properties of the base-isolation system reported in Table 2: i.e. stiffness ratio (α_{Ke}); thickness (t_{HDRL}) and primary shape factor (S_{HDRL}) of the HDRL, assuming constant values of the diameter (D_{HDRL}= 53cm) and elastic modulus of the rubber (E= 5.12MPa); effective viscous damping ratios in compression ($\xi_{eVc,BI}$) and in tension ($\xi_{eVt,BI}$); effective compression ($K_{eV,c}$) and tension ($K_{eV,t}$) vertical stiffnesses and corresponding vertical viscous damping constants ($C_{eV,c}$ and $C_{eV,t}$). It should be noted that different fundamental vibration periods of the BIHV structures are obtained (see Table 2), assuming a constant value (i.e. $T_{BI,1H}$= 2.21s) in the horizontal direction. Further details are reported in a previous study [14].

Table 2: Design properties of the horizontal and vertical base-isolation system with HDBRs and HDRLs (units in kN, m and s)

α_{Ke}	$T_{BI,1V}$	t_{HDRL}	$S_{1,HDRL}$	$\xi_{eVc,BI}$	$\xi_{eVt,BI}$	$K_{eV,c}$	$K_{eV,t}$	$C_{eV,c}$	$C_{eV,t}$
2000	0.08	0.0114	6.46	0.033	0.050	262108560	314530272	39217	58826
1600	0.084	0.0155	4.75	0.033	0.050	209686849	314530272	37350	56025
1200	0.089	0.0195	3.77	0.033	0.050	157265136	314530272	35252	52877
800	0.100	0.0247	2.98	0.033	0.050	104843424	314530272	31374	47061
400	0.127	0.0388	1.90	0.033	0.050	52421711	314530272	24704	37056
200	0.167	0.0446	1.65	0.033	0.050	26210856	314530272	18787	28180
100	0.225	0.0583	1.26	0.033	0.050	13105428	314530272	13944	20916
50	0.309	0.0764	0.96	0.033	0.050	6552714	314530272	10153	15230

3 NUMERICAL RESULTS

The original fixed-base (FB) and retrofitted base-isolated (BI) hospital pavilions described in Section 2, with (BIHV) and without (BIH) vertical base-isolation, are examined with the aim of evaluating the vertical isolation ratio necessary when they are subjected to near-fault ground motions with notable vertical component. Eight values of the effective stiffness ratio (α_{Ke}) are considered for the BIHV structures, while α_{Ke} equal to 2400 is considered for the BIH structure. A purpose-built C++ code is used for NLTH analyses of the test structures, assuming a lumped plasticity model proposed in a previous work [16] for RC frame members of the superstructure. A two sub-element discretisation with the same length and uniformly distributed mass is used for beams, in order to take into account potential plastic behaviour at their mid-span sections. The Rayleigh damping matrix of the FB structure and BI superstructure is built with reference to their fundamental vibration periods in the horizontal and vertical directions, and assuming different viscous damping ratios (i.e. $\xi_{H,FB}$=5%, $\xi_{H,BI}$=2% and $\xi_{V,FB}$=$\xi_{V,BI}$=2%). A three-spring-three-dashpot model is adopted for predicting the horizontal and vertical nonlinear response of HDRBs, with and without HDRLs. Specifically, the reduction of shear stiffness is assumed for increasing values of lateral displacement and compressive axial load, while the dependence of the axial stiffness on the lateral displacement, in terms of axial shortening or lengthening due to second order geometric, is also taken into account [11]. The equivalent viscous damping of the base-isolation system is assumed function of the shear strain in the horizontal direction, whereas a constant value is considered in the vertical one.

A set of fifteen near-fault pulse-type earthquakes is extracted from the PEER database [13], selecting ground motions with a pulse-like waveform in the vertical component as resulting from the application of the variational mode decomposition technique [12]. They are scaled to match, on average, the elastic design response spectrum of acceleration for the horizontal component provided by the Italian seismic code at the life-safety (LS) limit state and for the subsoil class C (i.e. PGA_H=0.405g and S_H=1.095). In particular, the mean acceleration response of each earthquake spectrum is scaled through the application of the same scale factor (SF) to

both horizontal components. Then, a mean spectrum of the fifteen earthquakes is obtained, whose values are within the 90% (lower limit) and the 130% (upper limit) of the 5% damped elastic design response spectrum in the range of vibration periods from $T_{min}=0.2T_{BI,1H}$ to $T_{max}=1.2T_{BI,1H}$ [9]. Main data of the selected earthquakes are reported in Table 3: i.e. year; recording station; moment magnitude (M_w); closest distance (Δ); peak ground accelerations along the horizontal (PGA_{H1} and PGA_{H2}) and vertical (PGA_V) directions; scale factor (SF). It is worth noting that the same SF value is applied for the horizontal and vertical components.

Table 3: Main data of the selected pulse-type near-fault records [13] (units in km and g)

Earthquake	Year	Station	M_w	Δ	PGA_{H1}	PGA_{H2}	PGA_V	SF
Gazli	1976	Karakyr	6.8	5.5	0.702	0.864	1.698	0.60
Imperial Valley	1979	EC County Center	6.5	7.3	0.212	0.235	0.245	0.75
Imperial Valley	1979	El Centro Array #5	6.5	4.0	0.529	0.383	0.594	1.00
Imperial Valley	1979	El Centro Array #6	6.5	1.4	0.447	0.449	1.895	0.40
Imperial Valley	1979	El Centro DA	6.5	5.1	0.481	0.353	0.770	1.00
Irpinia	1980	Sturno (STN)	6.9	10.8	0.227	0.321	0.235	1.00
Loma Prieta	1989	Gilroy Array #2	6.9	11.1	0.370	0.323	0.295	1.15
Loma Prieta	1989	Saratoga (AA)	6.9	8.5	0.514	0.326	0.396	1.10
Northridge-01	1994	LA Dam	6.7	5.9	0.426	0.324	0.319	1.05
Northridge-01	1994	Newhall (WPC)	6.7	5.5	0.419	0.357	0.296	0.85
Kobe	1995	Takarazuka	6.9	0.3	0.697	0.614	0.427	0.90
Chi-Chi	1999	TCU068	7.6	0.3	0.512	0.371	0.530	0.60
Duzce	1999	Duzce	7.1	6.6	0.404	0.515	0.346	1.00
Chuetsu-oki	2007	Kariwa	6.8	12.0	0.360	0.475	0.409	0.60
Darfield	2010	LINC	7.0	7.1	0.461	0.388	0.915	1.00

Firstly, mean of maximum values of the ductility ratio ($\alpha_\mu=\mu_{\chi,max}/\mu_{\chi u}$, being $\mu_{\chi,max}$ and $\mu_{\chi,u}$ maximum and ultimate values of the curvature ductility, the latter evaluated as proposed in [17]) at all levels of FB, BIH and BIHV structures is plotted in Figure 3. Plots refer to the mid-span section of central beams of the interior frame along Y direction characterized by the greatest vertical tributary area (see Figure 1). Moreover, values of the effective stiffness ratio ($\alpha_{Ke}=K_{eV}/K_{eH}$) and corresponding vertical isolation ratio ($\alpha_T=T_{BI,1Z}/T_{FB,1Z}$) are reported for each structure. Note that NLTH analyses are prematurely stopped when cavitation load ($F_c=3GA_o$, where G and A_o represent the shear rubber modulus and the bonded rubber area at onset of cavitation, respectively [18]) of HDRBs and ultimate curvature ductility at the mid-span section of all beams ($\alpha_\mu=1$) are attained. For the sake of comparison, the minimum final instant of simulation is considered for all α_{Ke} values.

Figure 3 describes the effect of the vertical isolation, with maximum values of the ductility ratio recorded at the upper two levels of the FB (dashed black line) and BIH (solid black line), reaching $\alpha_{\mu,FB} \cong 0.9$ and $\alpha_{\mu,BI} \cong 0.6$ at the roof level. The ductility ratio decreases for decreasing α_{Ke} values for the BIHV structures, moving from a maximum top value of 0.55 for $\alpha_{Ke}=2000$ (i.e. $\alpha_T=1.21$, violet line) to a minimum top value slightly greater than 0.1 for $\alpha_{Ke}=50$ (i.e. $\alpha_T=4.68$, green line). Moreover, the trend towards an almost constant distribution of α_μ along the building height confirms that the structure above the isolators can be considered as isolated along the vertical direction.

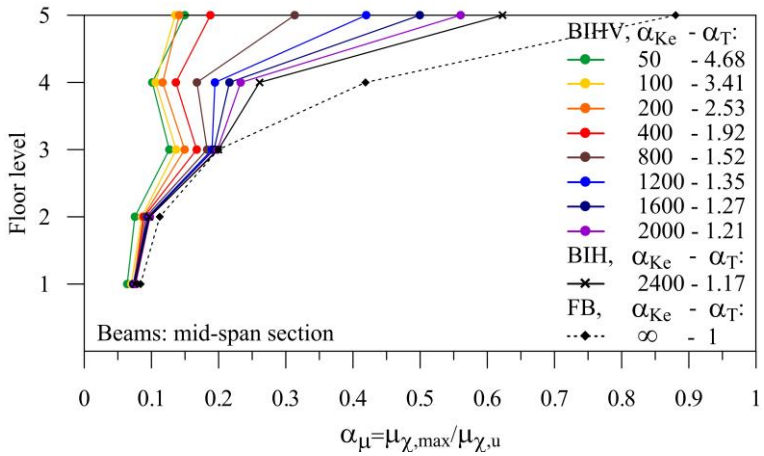

Figure 3: Mean of maximum ductility ratios of the BIHV, BIH and FB structures

Graph similar to the previous one is shown in Figure 4, where maximum vertical acceleration (a_V) at the same mid-span sections considered for the maximum ductility demand is assumed as representative of the seismic damage for acceleration sensitive nonstructural elements. The effectiveness of the vertical seismic isolation is verified checking when the peak floor vertical acceleration threshold imposed by the current Italian standard [17] is not reached (dashed black line). As can be observed, this limitation of the maximum vertical floor acceleration is satisfied at all levels of the BIHV structures characterized by $\alpha_{Ke}<400$.

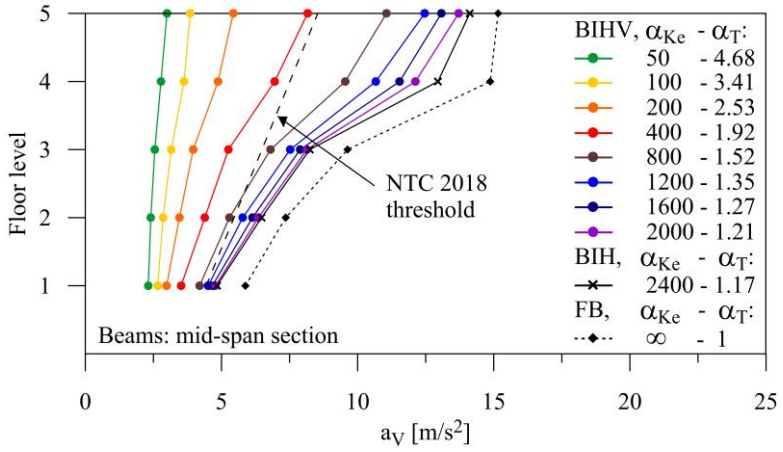

Figure 4: Mean of maximum vertical accelerations of the BIHV, BIH and FB structures

Afterwards, a simplified five-step design procedure of the vertical isolation ratio (α_T) is developed on the basis of NLTH and LTH analyses of the test structures, the latter performed assuming an elastic behaviour of both superstructure and base-isolation system. Specifically, time histories of vertical acceleration at the mid-span section of beams are investigated by wavelet analysis, providing information on the frequency content of the seismic signal over time and also assessing the occurrence of vertical moving resonance effects when the nonlinear seismic response is considered. A Matlab code is implemented in order to obtain the wavelet transform coefficient (WTC) in the time (t) – vertical vibration period (T_V) domain, using the continuous wavelet transform algorithm in combination to the complex Morlet wavelet [14]

$$WTC = \frac{1}{\sqrt{|s|}} \int_{-\infty}^{+\infty} a_V(t) \cdot \psi^* \left(\frac{t-\tau}{s} \right) dt \tag{1}$$

where s is the inverse of the frequency and ψ^* is the complex conjugate of the wavelet function ψ. Then, the wavelet transform integral coefficient (WTIC) is assumed as representative of the amount of input energy [19]

$$WTIC = \int_{t_0}^{t_f} \int_{T_{V,\min}}^{T_{V,\max}} WTC(t, T_V) \cdot dT_V \cdot dt \tag{2}$$

where the initial (t_0) and the final (t_f) instants of the time history are reported together with the range of vertical vibration periods (i.e. $T_{V,min}=0.2 \cdot T_{1V}$ and $T_{V,max}=2 \cdot T_{1V}$) provided by Eurocode 8 [20]. It should be noted that $T_{V,max}=1 \cdot T_{1V}$ is assumed for LTH analysis, since no elongation of the fundamental vibration period in the vertical direction is expected when elastic behaviour is considered. For all the examined cases, the final instant of NLTH analyses is reached earlier once the cavitation force of HDRBs and ultimate ductility demand of mid-span section of beams are attained, while the total duration of the records is always considered for LTH analyses.

As first step, in Figure 5 curves representing the vertical isolation ratio (α_T), at the first (red line), third (blue line) and fifth (black line) level, are reported against the ductility ratio (α_μ), thus allowing evaluation of the α_T value corresponding to a target damage threshold. A notable decrease of α_μ with increasing vertical isolation is resulted at the roof level, while only a slight influence of α_T is highlighted at the other floor levels with an almost constant value of α_μ.

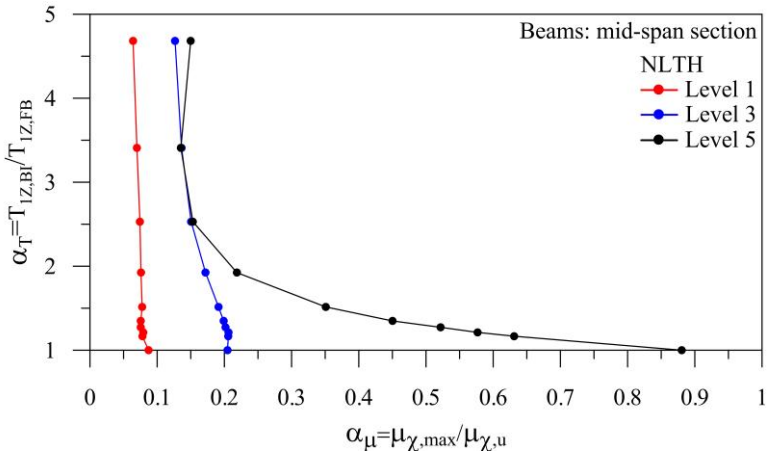

Figure 5: First step of the vertical isolation ratio design procedure

As an example, the response of the superstructure at the mid-span sections of beams proves to be practically elastic (e.g. α_μ=0.2) at all levels assuming an isolation ratio α_T=2.

Then, a plane correlation based on a regression analysis of the nonlinear dynamic results is reported in the logarithmic space (Figures 6a,c,e), for predicting the vertical acceleration (a_V) at the mid-span section of beams as function of α_μ and α_T values evaluated in the first step.

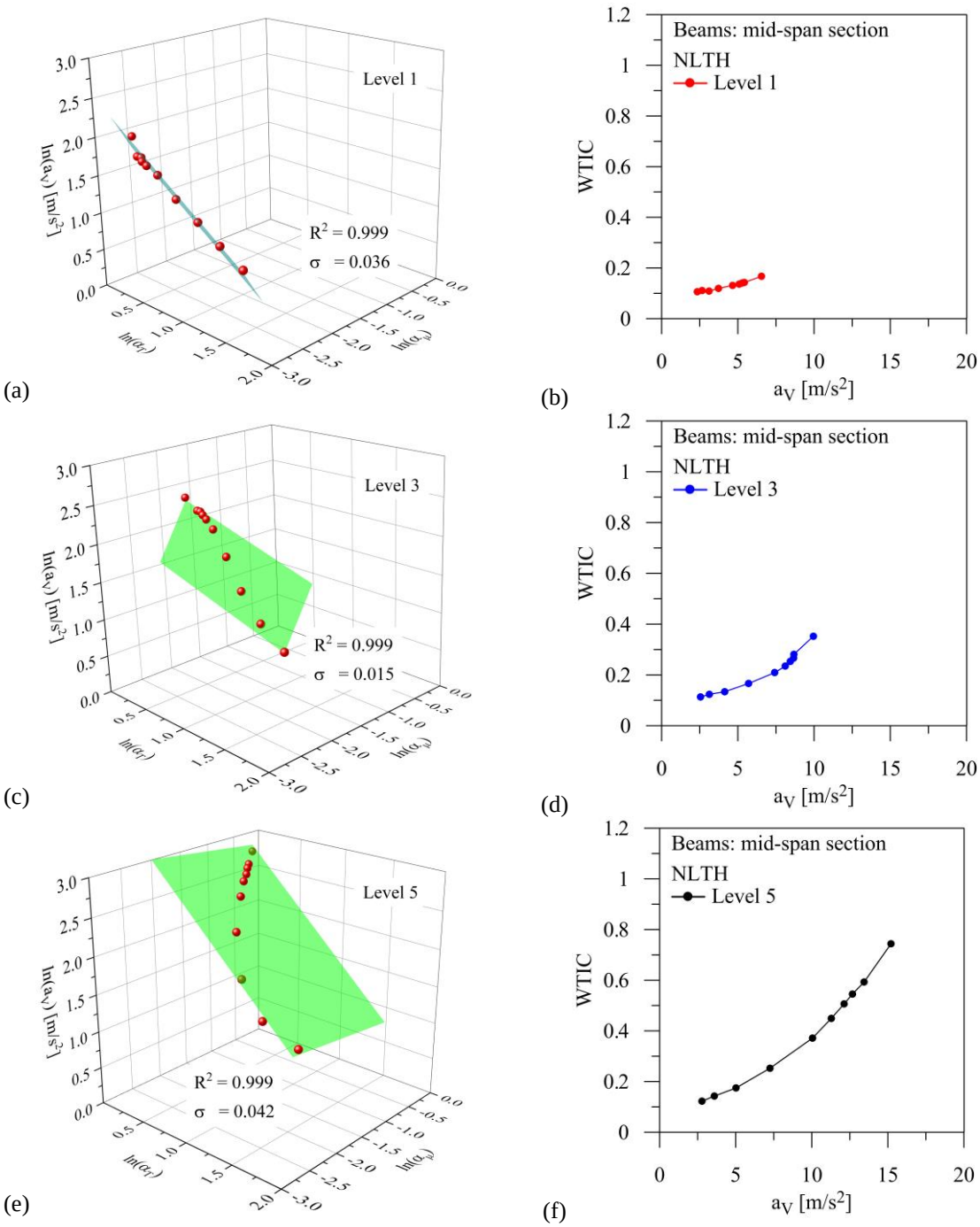

Figure 6: Second (a, c, e) and third (b, d, f) step of the vertical isolation ratio design procedure

A good correlation is highlighted at all levels, with a coefficient of determination (R^2) equal to 0.999 and standard error of residuals (σ) ranging from a minimum of 0.015 (Figure 6c) to a maximum of 0.042 (Figure 6e). Then, WTIC value related to the vertical isolation ratio resulting from the first step is evaluated through Equation 2 and represented in Figures 6b,d,f depending on the vertical acceleration derived in the second step. Note that WTIC increases for increasing values of a_V, quickly reaching the highest value at the roof level (Figure 6f).

Afterwards, the variability of WTIC with the vertical isolation ratio is depicted in Figure 7 with reference to NLTH (solid line) and LTH (dotted line) analyses. A significant difference between WTIC values is observed at level 5 (black lines), especially when FB (α_T=1) and BIH (α_T=1.17) and BIHV (α_T=1.21 and α_T=1.27) structures are considered. This result highlights the highest input energy obtained with the assumption of elastic behaviour. Moreover, gap between WTIC values obtained from LTH and NLTH analyses tends to decrease for increasing values of α_T, proving the effectiveness of base-isolation in the vertical direction.

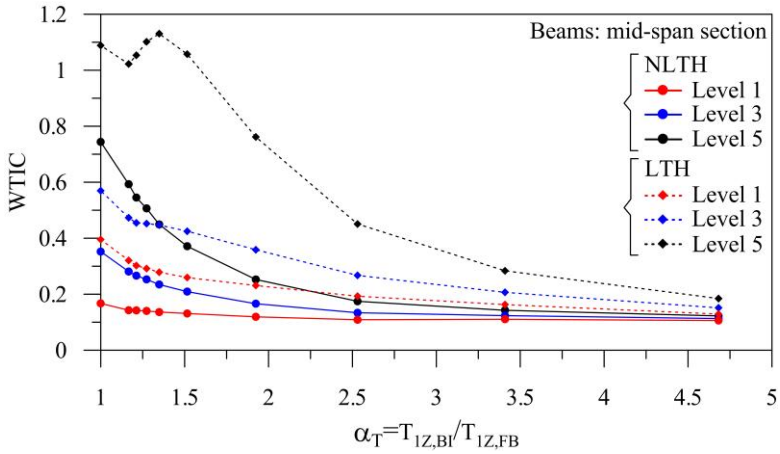

Figure 7: Fourth step of the vertical isolation ratio design procedure

As fifth step, the variability of the vertical isolation ratio (α_T) resulting from LTH (blue line) and NLTH (black line) analyses, together with their difference ($\Delta\alpha_T$, red line), is reported in Figure 8 in terms of the ductility ratio (α_μ).

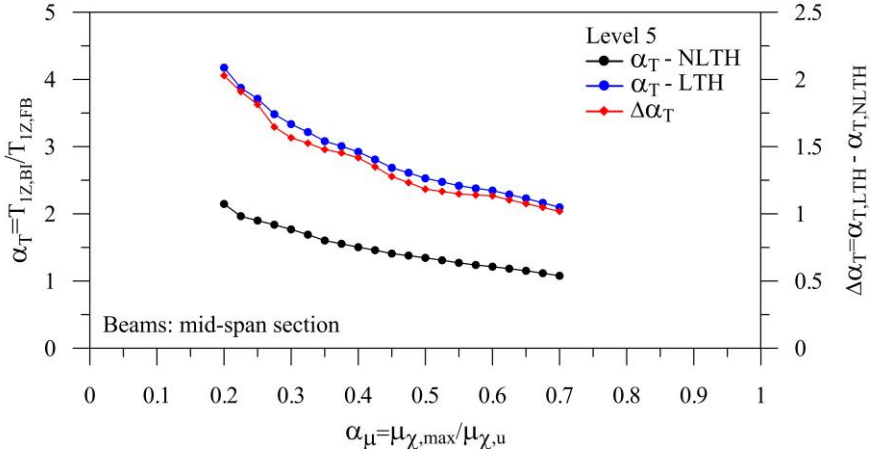

Figure 8: Fifth step of the vertical isolation ratio design procedure

It is worth noting a significant difference between the vertical isolation ratio required by NLTH and LTH analyses, with its high overestimation when elastic behaviour is hypothesized. This suggests that the lower the ductility ratio demand, the higher the need to use a corrective factor ($\Delta\alpha_T$) of LTH results, reducing from a maximum value $\Delta\alpha_T \cong 2.0$ for $\alpha_\mu=0.20$, to a minimum value $\Delta\alpha_T \cong 1.0$ for $\alpha_\mu=0.7$.

4 CONCLUSIONS

The proposal of a simplified design procedure of the vertical isolation ratio required to obtain an effective protection of RC framed structures, with regard to the vertical component of near-fault earthquakes, is the main goal of this study. To this end, elastic LTH results are calibrated starting from those deriving from inelastic NLTH ones by means of wavelet analysis providing a good representation of the effects of spectral nonstationarity and vertical moving resonance on the structural response. Computation of a wavelet transform integral coefficient is carried out as to be representative of the total seismic input energy over the time and in a significant range of vertical vibration periods. A fixed-base five-storey RC hospital building is retrofitted by means of horizontal and vertical base-isolation system, deriving from an in-series vertical assembly of a HDRB and a HDRL only function of the compressive axial load. Eight values of the vertical-to-horizontal stiffness ratio of the base-isolation system are considered, assuming different values for the vertical stiffness of the HDRL. An extensive numerical investigation is carried out employing a set of fifteen near-fault earthquakes with pulse-type behaviour in the horizontal and vertical directions. Vertical base-isolation is effective for reducing both ductility and vertical acceleration demands at the mid-span section of beams, especially at the upper levels of the superstructure, confirming to be a reliable solution for the seismic protection of structural and acceleration-sensitive nonstructural elements. The significant difference observed between the vertical isolation ratio resulting from NLTH and LTH analyses highlights that a too high overestimation of its value may be necessary when elastic structural behaviour is hypothesized. This suggests the introduction of a corrective factor of the vertical isolation ratio deriving from LTH analysis, whose value increases for decreasing values of the target ductility demand.

ACKNOLEDGEMENTS

The present work was financed by Re.L.U.I.S. (Italian network of university laboratories of earthquake engineering), in line to the Convenzione D.P.C.-Re.L.U.I.S. 2024–2026, WP15, Devices and systems of Isolation and Dissipation.

REFERENCES

[1] Mazza, F., A. Donnici, and R. Labernarda. 2024. Structural and non-structural numerical blind prediction of shaking table experimental tests on fixed-base and base-isolated hospitals. Earthquake Engineering and Structural Dynamics, 53(10): 2961-2987.

[2] Mazza, F. 2016. Effects of near-fault vertical earthquakes on the nonlinear incremental response of r.c. base-isolated structures exposed to fire. Bulletin of Earthquake Engineering, 14(2): 433-454.

[3] Di Sarno, L., A. S. Elnashai, and G. Manfredi. 2011. Assessment of RC columns subjected to horizontal and vertical ground motions recorded during the 2009 L'Aquila (Italy)

earthquake. Engineering Structures, 33:1514-1535.
[4] Naga, P., and M. R. Eartherton. 2014. Analyzing the effect of moving resonance on seismic response of structures using wavelet transforms. Earthquake Engineering and Structural Dynamics, 43:759-768.
[5] Zhou, Z., J. Wong, and S. Mahin. 2016. Potentiality of using vertical and three-dimensional isolation systems in nuclear structures. Nuclear Engineering and Technology, 44:1237-1251.
[6] Liu, W. G., H. Xu, W. F. He, and Q. R. Yang. 2018. Static test and seismic dynamic response of an innovative 3D seismic isolation system. Journal of Structural Engineering, 144(12): 04018212.
[7] Pourmasoud, M. M., J. B. P. Lim, I. Hajirasouliha, and D. McCrum. 2020. Multi-directional base isolation system for coupled horizontal and vertical seismic excitations. Journal of Earthquake Engineering, 26(3): 1-26.
[8] Vu, B., M. Unal, G. P. Warn, and A. M. Memari. 2014. A distributed flexibility and damping strategy to control vertical accelerations in base-isolated buildings. Structural Control and Health Monitoring, 21:503-521.
[9] Eurocode 8. 2005. *Design of structures for earthquake resistance – part 2: bridges*. Comité Européen de Normalisation (CEN), Brussels, Belgium.
[10] EN15129. 2009. *Antiseismic Devices*. Comité Européen de Normalisation (CEN), Brussels, Belgium.
[11] Mazza, F., and R. Labernarda. 2021. Internal pounding between structural parts of seismically isolated buildings. Journal of Earthquake Engineering, 26(10): 5175–5203. https://doi.org/10.1080/13632469.2020.1866122.
[12] Quaranta, G., G. Angelucci, and F. Mollaioli. 2022. Near-fault earthquakes with pulse-like horizontal and vertical seismic ground motion components: analysis and effects on elastomeric bearings. Soil Dynamics and Earthquake Engineering, 160:107361.
[13] Pacific Earthquake Engineering Research Center database, PEER. 2004. https://ngawest2.berkeley.edu/
[14] Mazza, F., and A. Braile. 2024. Vertical isolation ratio of base-isolated RC structures subjected to near-fault earthquakes. Procs. of the 18th World Conference on Earthquake Engineering, 30th June – 5th July, Milan, Italy.
[15] DM96. 1996. *Norme tecniche per le costruzioni in zone sismiche e relative istruzioni, D.M. 16-01-1996 and C.M. 10-04-1997*. Ministero dei Lavori Pubblici, Rome, Italy.
[16] Mazza, F. 2021. Base-isolation of a hospital pavilion against in-plane-out-of-plane seismic collapse of masonry infills. Engineering Structures, 228:111504.
[17] NTC2018. 2018. *Norme tecniche per le costruzioni e relative istruzioni, D.M. 17-01-2018 and C.M. 11-02-2019*. Ministero delle Infrastrutture e dei Trasporti, Rome, Italy.
[18] Kumar, M., A. S. Whittaker, and M. C. Constantinou. 2014. An advanced numerical model of elastomeric seismic isolation bearings. Earthquake Engineering & Structural Dynamics, 43(13): 1955–1974.
[19] Li, H., T. Yi, M. Gu, and L. Huo. 2009. Evaluation of earthquake-induced structural damages by wavelet transform. Progress in Natural Science 19: 461–470.
[20] Eurocode 8. 2004. *Desing provisions for earthquake resistance of structures – part 1: general rules, seismic actions and rules for buildings*. Comité Européen de Normalisation (CEN), Brussels, Belgium.